

## Full paper

# Rationally designed sea snake structure based triboelectric nanogenerators for effectively and efficiently harvesting ocean wave energy with minimized water screening effect

Steven L. Zhang<sup>a,1</sup>, Minyi Xu<sup>a,b,1</sup>, Chunli Zhang<sup>a,c,1</sup>, Yi-Cheng Wang<sup>a</sup>, Haiyang Zou<sup>a</sup>, Xu He<sup>a</sup>, Zhengjun Wang<sup>a</sup>, Zhong Lin Wang<sup>a,d,\*</sup>

<sup>a</sup> School of Materials Science and Engineering, Georgia Institute of Technology, Atlanta, GA 30332-0245, United States

<sup>b</sup> Marine Engineering College, Dalian Maritime University, Dalian 116026, China

<sup>c</sup> Department of Engineering Mechanics, Zhejiang University, Hangzhou, Zhejiang 310027, China

<sup>d</sup> Beijing Institute of Nanoenergy and Nanosystems, Chinese Academy of Science, Beijing 100085, China

## ARTICLE INFO

## Keywords:

Blue energy  
Triboelectric nanogenerators  
Energy harvesting  
Electrostatic screening  
Self-powered systems

## ABSTRACT

Ocean waves are one of the most power dense energy sources in the environment. Triboelectric nanogenerators (TENGs) have been demonstrated to effectively harvest mechanical energy carried by low frequency, random/irregular actuation, such as from ocean waves. In this work, a novel design of triboelectric nanogenerator based on the Pelamis snake energy harvester is presented. The sea snake based TENG, with its lightweight structure, was able to harvest energy effectively at low amplitude ocean wave by utilizing charged polytetrafluoroethylene balls that would roll due to the wave's curvature. With the integration of springs to connect different segments, the segments are able to bend easily, allowing the enclosed balls to move faster, producing higher output power. The design of an air gap structure allows each segments of the sea snake based TENG to minimize electrostatic induction from ions in sea water, and solve the effect of dielectric shielding from the water on the device performance, as the water, if it is close to the TENG's electrodes, has a detrimental effect causing an increase of the TENG's internal capacitance, which would result in a low voltage with the same amount of charge being transformed. Thus, this illustrates the importance of the air gap structure to minimize low voltage due to high internal capacitance. This further shows the sea snake based triboelectric nanogenerator could be used in actual ocean conditions, such as in high salinity water environment. The added tapered spring to replace the air gap was able to allow the balls on the TENG to move more quickly, as it increased the rotational angle, and the TENG has a maximum power density of  $3 \text{ W/m}^3$  under actuation. Due to the minimization of dielectric shielding of device performance, the sea snake TENG exhibits a high voltage in simulated water wave conditions.

## 1. Introduction

Due to the dwindling supply of nonrenewable fossil fuels and an increase in world energy consumption in the past decades, intensive research efforts are being devoted into the development of alternative renewable and clean energy technologies [1–3]. One method is to harvest mechanical energy from the ambient environment as it could supplement the energy needs due to its great abundance and ubiquity. One form of mechanical energy from the ambient environment comes from the ocean, as it is one of the most power dense form of energy, that could be harvested [4–8]. Harvesting energy from water waves displays many advantages, such as it is always present, and is independent of

time of day, weather, or seasons [9,10]. Currently, most commercial ocean wave energy harvesters consists of electromagnetic generators (EMGs) [11]. However, the main technology of these generators is a permanent magnet, which makes the device heavy, bulky, and costly, making the EMGs difficult to be mass produced, hindering most production of ocean wave energy harvesters. Also, the heaviness of the structure would increase the damping factor, as it requires a larger wave to move the structure, causing most energy to be not effectively harvested [12]. Most importantly, the low driving frequency from the water wave made the output of EMG so low, as the output power of the EMG is proportional to frequency squared [12], that it is hardly used for driving any reasonable size of electronics, and technology have been

\* Corresponding author.

E-mail addresses: [stlzhang@gatech.edu](mailto:stlzhang@gatech.edu) (S.L. Zhang), [zhong.wang@mse.gatech.edu](mailto:zhong.wang@mse.gatech.edu) (Z.L. Wang).

<sup>1</sup> These authors contributed equally to this work.

used to upconvert the frequency of the wave to obtain the desired power rating for EMG, which requires additional area. Thus, a new technology that is lightweight, small sized, and cost effective, is needed to harvest energy from the ocean wave effectively.

Recently, nanogenerators, in particular, piezoelectric nanogenerators and triboelectric nanogenerators (TENG), has been developed as a low cost and effective way to harvest energy from an ambient environment especially for energy with random amplitude and low frequency [13–35]. The main mechanism of the TENG is based on contact electrification and electrostatic induction, and recently the TENG's fundamental physics has been attributed to Maxwell's displacement current [36]. TENGs also show far superior outputs than EMG for harvesting energy from the ocean, as it is more effective in harvesting energy from low frequency, as for TENG, the output power is directly proportional to the frequency, which typical ocean waves are, with frequencies of  $< 1$  Hz [12,21,22,37]. So far, different designs of triboelectric nanogenerators have been explored to harvest energy from water waves [9,21–23,25,38–42]. However, charges from the ionicity of the ocean's salt water and the environment's humidity both have a negative effect of the triboelectric performance. Full packaging of the device was able to solve only the effect of humidity on the triboelectric performance, but has not solved the effect of dielectric shielding in the ocean in this device. Thus, new research is needed to address the problem of dielectric shielding, causing a lower device's output performance.

In this work, a novel design of TENG based on rolling electrification, a type of contact electrification, and electrostatic induction is presented. The TENG consists of multiple segments that are connected with springs. The springs allow it to have an external restoring force acting on the segments, which would greatly enhance the performance of the TENG by increasing the ball's velocity, as the displacement of the segments is increased. The TENG was also based of the Pelamis Snake Energy Harvester, the first offshore energy harvester to generate electricity into the grid. For the Pelamis Snake Energy Harvester, the device could harvest power with high amplitude wave (6 m tall), due to its bulky and heavy structure (mass of each segments weighing 70 t each), and thus a new structure is needed to harvest energy effectively at low amplitude and low frequency waves [43,44]. The sea snake based triboelectric nanogenerator (SS-TENG) structure use the advantage of

connected section, which are able to flex and bend easily due to the lightweight elements of the triboelectric nanogenerators as a wave pass through, and is the first TENG to harvest energy from the wave's curvature. The SS-TENG could also harvest energy effectively from the horizontal movement of the device caused by the wave. The design of an air gap structure in the segment of the sea snake based triboelectric nanogenerator (SS-TENG) was incorporated to minimize and solve the capacitive effect from the water, which has a negative effect on the device performance, showing the SS-TENG could operate in simulated ocean conditions, such as in high salinity water environment. The added tapered spring to fill the air gap further increased the operating angle of the device, thus increasing the performance of the TENG, as the TENG has a maximum power density of  $3 \text{ W/m}^3$  under linear motor actuation to simulate ocean waves. The SS-TENG could be easily to be fabricated, making it a cost-effective and sustainable ocean wave energy harvester.

## 2. Results/discussion

### 2.1. Structure and working principle of SS-TENG

A schematic structure of SS-TENG in an ocean energy farm is shown in Fig. 1a. A segment of the SS-TENG is shown in Fig. 1b, and the detailed fabrication process is explained in the experimental section. The interior of the sea snake is comprised of polytetrafluoroethylene (PTFE) balls, Nylon film, sputtered copper layer, and a soft tapered spring, which is shown in Fig. 1c, which is the zoomed in schematic of the cross-section of the SS-TENG. The copper was also arranged in an interdigital way to increase the frequency of the balls rolling across the electrode, which would increase the overall output current of the device [41]. The exterior consists of an acrylic box, acting as a packaging element, which prevents water from entering the device, and an exterior spring to enhance movement of segments with the balance force to enhance the energy harvested. The spring acts in a way that it stores the potential energy and further acts on the segments of the sea-snake, providing a restoring spring force acting on the segments, for it to easily move, increasing the net displacement of the segments.

The working mechanism for the SS-TENG is shown in Fig. 1d. Under an external triggering, such as a water wave move across the acrylic

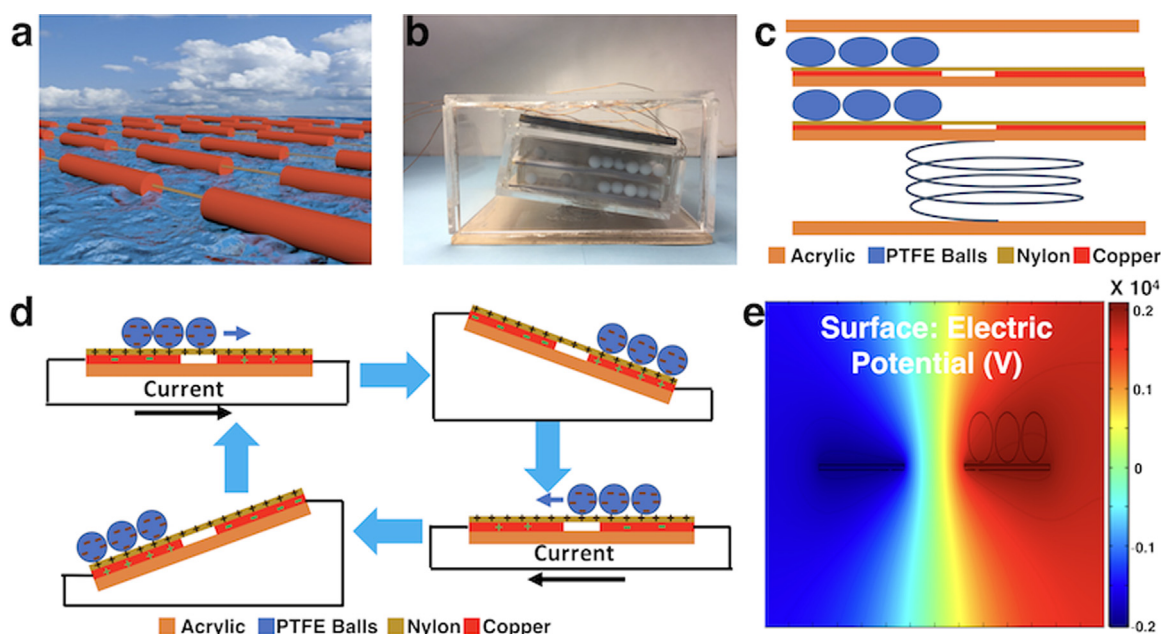


Fig. 1. (a) Array of sea snake triboelectric nanogenerators on an ocean energy farm. (b) Digital photo of a single segment of the SS-TENGs (c) cross sectional schematic of the SS-TENG. (d) The working mechanism of the SS-TENG. (e) The simulated electric potential distribution induced by the rolling PTFE balls.

structure, the springs attaching the acrylic boxes would bend due to the curvature of the incoming water wave. In turn, the acrylic boxes would be inclined, causing the balls to roll down the nylon film. After the first contact, the PTFE balls would become negatively charged due to contact electrification with the thin film. While the balls are sliding down, they would induce positive charges on the bottom left electrode (in Fig. 1d), which would produce a current to flow onto the upper electrode. Furthermore, after the water wave move past the acrylic structure, the SS-TENG structure would be inclined in the other direction. This is similar to energy harvesting of the duck shaped triboelectric nanogenerator [42], but with the additional spring, the instantaneous frequency is upconverted, causing an increase in current and power. This would allow the PTFE balls to roll down in the other direction, which would produce electricity in the bottom right electrode, producing a net current in the opposite direction. Overall, this design is a freestanding rolling mode triboelectric nanogenerator, as the balls act as a dielectric layer above the electrodes, and due to the movement of the balls, there exist a charge transfer between the electrode. Furthermore, a finite element model simulation was used to simulate the potential, and the result could obtain up to 4000 V, as shown in Fig. 1e.

According to the theory behind the freestanding sliding mode TENG, there exists a relationship between the charge density  $\sigma$ , infinitesimal small segments of the top dielectric layer  $dk$ , the width of top dielectric layer  $w$ , the total length of the dielectric layer  $l$ , the capacitance between dielectric surface and left electrode  $C_1(k)$ , and the capacitance between dielectric surface and right electrode  $C_2(k)$ , the  $x(t)$ , the position of the dielectric layer at a function of time, and the  $Q_{sc}$  as shown in Eq. (1) below [45],

$$Q_{sc} = \int_0^l \frac{\sigma w dk}{1 + \left(\frac{C_2(k)}{C_1(k)}\right)_{x=g+l}} - \int_0^l \frac{\sigma w dk}{1 + \left(\frac{C_2(k)}{C_1(k)}\right)_{x=0}} \quad (1)$$

As shown in Eq. (1),  $Q_{sc}$  reaches its maximum when  $x = 0$ , or  $x = g + l$ , in which  $Q_{sc}$  is  $\sigma w l$ , where  $C_2(k)$ , or  $C_1(k) = 0$ . Also, it is important to note that there is a relationship between the maximum short circuit charge  $Q_{sc,max}$  and the output open circuit voltage  $V_{oc,max}$ ,

and the capacitance between the electrodes  $C_0$  as shown in Eq. (2) below,

$$V_{oc,max} = \frac{Q_{sc,max}}{C_0} = \frac{\sigma w l}{C_0} \quad (2)$$

Therefore, the performance of the SS-TENG can be optimized by choosing proper materials for the dielectric layer, such as using electret material, which is able to store charge on the surface to maximize the charge density  $\sigma$ , like PTFE balls, when the PTFE is fully charged. It is also needed to maximize the number of balls to increase the area ( $w \cdot l$ ) to obtain the maximum  $Q_{sc,max}$ , which would increase  $V_{oc}$ . Another way to maximize  $V_{oc}$  is to maintain a low capacitance  $C_0$  in between the two electrodes. This would be used further in the article in the discussion of the effect of water increasing  $C_0$ . Also, it is necessary to note that the performance is independent of the film structure, and the output charge is evaluated by utilizing different materials, such as Kapton, PTFE film, nylon, or no film, as shown in Supplementary material Fig. S1. The reason nylon film was chosen, was that it is a good packaging materials, and it is able to protect delamination of the thin copper electrode when the PTFE balls move across them, and it has the highest output, due to it's more likely to lose electrons, as it is more positive on the triboelectric series.

## 2.2. Performance of SS-TENG

The electrical characteristic of the single segment of the SS-TENG without the use of spring under the regular motion of the rocker is shown in Fig. 2. The single segment of SS-TENG has a rectangular shape with a width of 2 in. (5.1 cm), length of 2.5 in. (6.4 cm), and height of 1 in. (2.54 cm) was placed on top of the rocking platform, as shown in Fig. 2a. The rocking platform moves back and forth, being inclined in one direction, and then inclined in the other direction at a low frequency (frequency < 0.5 Hz) to simulate the ocean wave movement conditions. The SS-TENG currently has  $N$  number of layers and  $N$  number of balls per each column. It currently has a total of 6 columns spaced evenly of 0.28 in. and has 5 separators spaced evenly with width

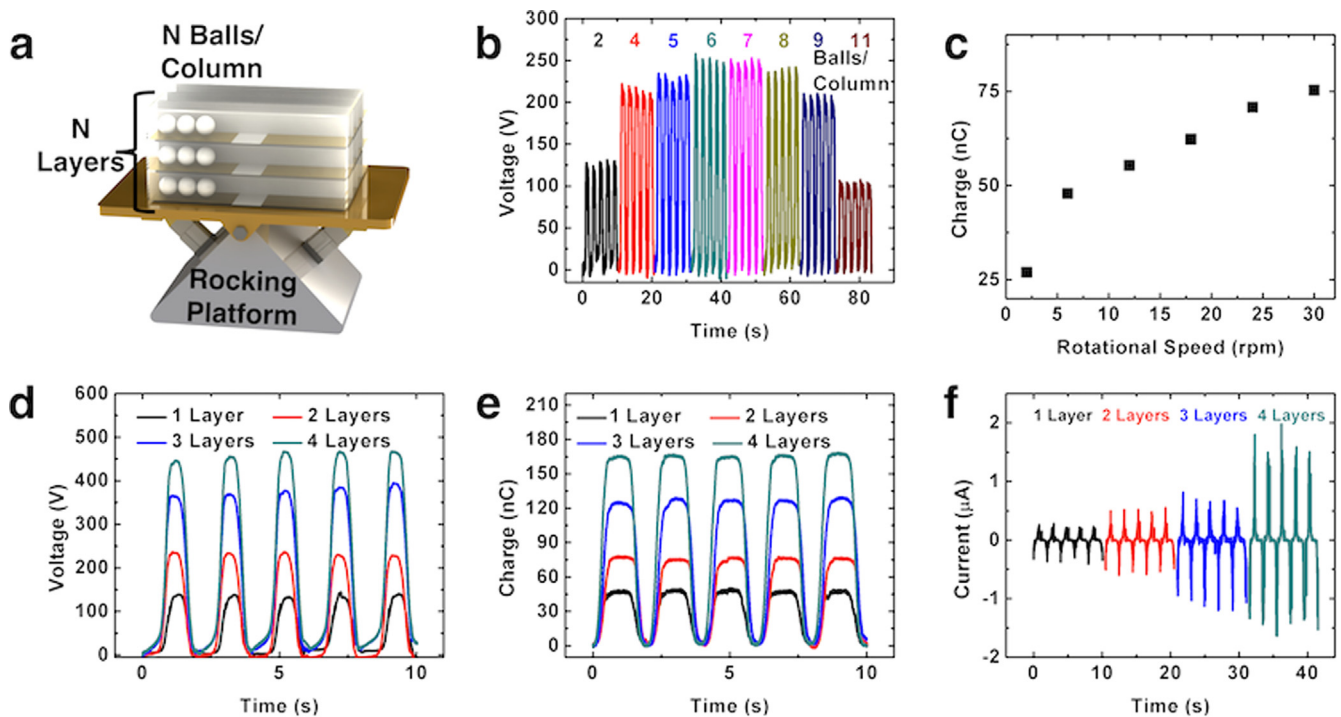


Fig. 2. Electrical performance of the SS-TENG by a laboratory rocking platform. (a) The 3D schematic of the SS-TENG on the rocking platform. (b) Dependence of voltage vs time with different balls/column. (c) Charge vs rotational speed of the rocking platform. (d) Voltage vs time at different layers. (e) Charge vs time at different layers. (f) Current vs time at different layers.

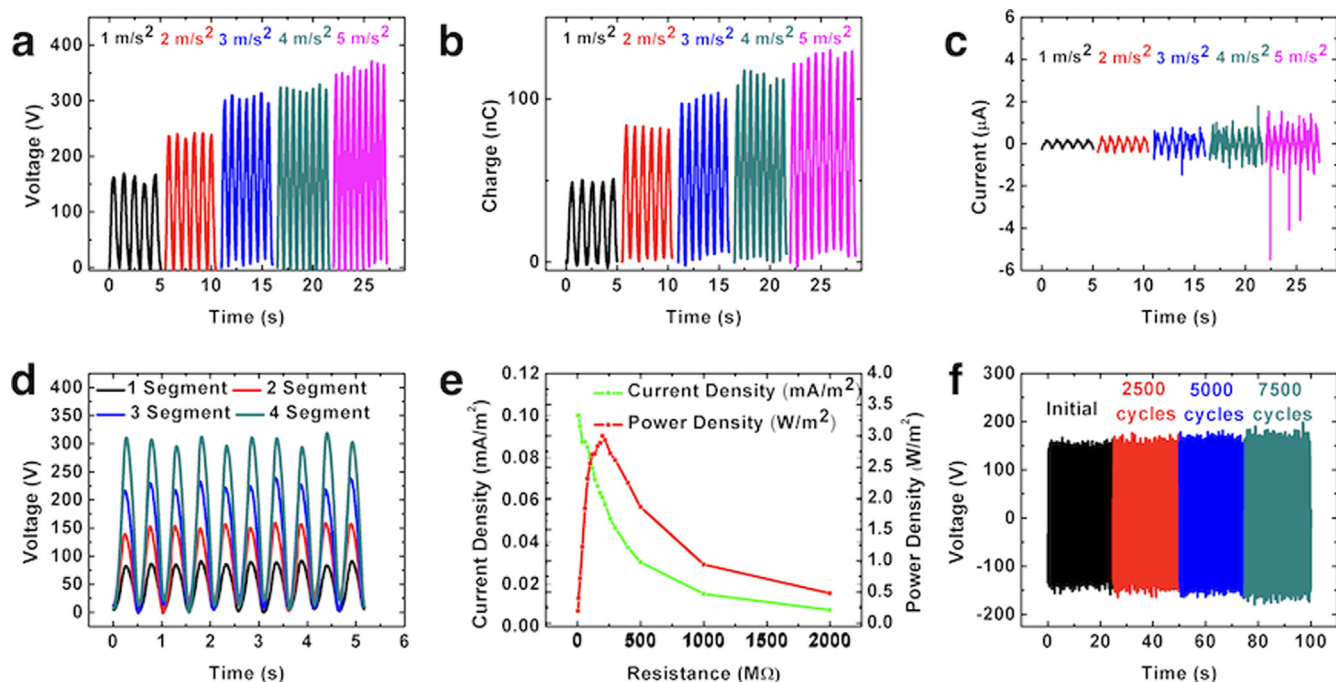


Fig. 3. Electrical performance of the SS-TENG by a linear motor (a) voltage vs time at different acceleration of a SS-TENG with two layer. (b) Charge vs time at different acceleration of a SS-TENG with two layer. (c) Current vs time at different acceleration of a SS-TENG with two layer. (d) Performance of sea snake TENG with multiple segments at acceleration of 1 m/s<sup>2</sup>. (e) Power density and current density dependence of resistance for 2 segments of SS-TENG with acceleration of 3 m/s<sup>2</sup>. (f) Electrical durability of SS-TENG over various cycles.

of 0.06 in. First, an optimization step is needed to measure the number of PTFE balls with a diameter of 0.25 in. (0.64 cm) that are needed per column to produce the maximum output. This is done in Fig. 2b, with two layers filled with different balls per column. The maximum output

voltage is measured at 6 balls/column, corresponding to 50% of area are filled with balls. Six balls/column would be used as a standard for all layers. Further, the effect on charge due to different rotational speed of the shaker has been evaluated, and the charge increase linearly with

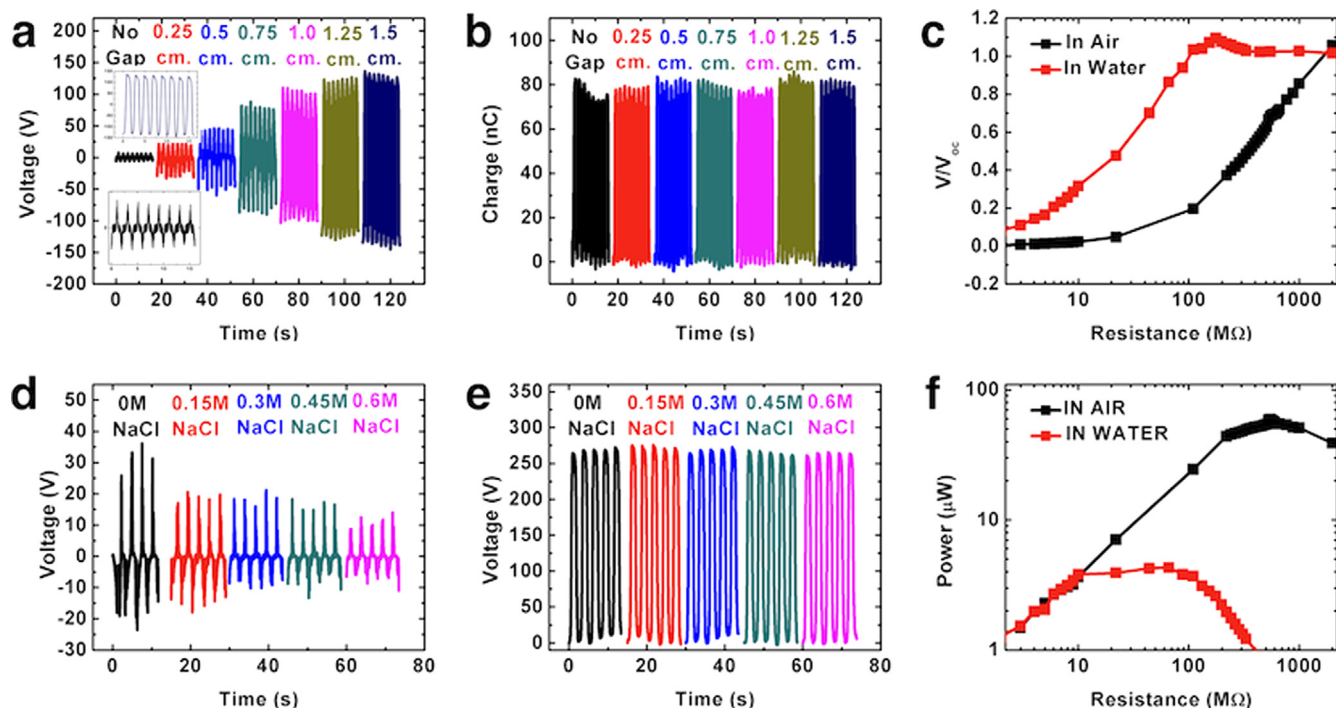


Fig. 4. Electrical performance of the SS-TENG in water and in air. (a) Voltage vs time comparison with SS-TENG with different air gap's height. Top inset: the zoomed in of output voltage with air gap of 1.5 cm. Bottom inset: zoomed in of output voltage with no air gap. (b) Charge vs time comparison with SS-TENG with different air gap's height. (c) Comparison of actual voltage/V<sub>oc</sub> with different resistance with SS-TENG with no air gap in air and in water. (d) Comparison of output power with different resistance with SS-TENG with no air gap in air and in water. (e) Voltage vs time of SS-TENG with air gap in water at different concentrations of NaCl. (f) Voltage vs time of SS-TENG without air gap in water at different concentrations of NaCl.

the rotational speed. This is due to the increase of speed causes the ball to move at a faster speed, having more kinetic energy that is converted into electrical energy. It is also necessary to note for low speeds, the ball only could be moved slightly due to the lack of kinetic energy to overcome the frictional force to slide fully down the nylon film; thus, at low speeds, there is a very low charge output.

Furthermore, the number of layers effect on the TENG was measured. Each layer refers to the effect of the previous layers included, as they are measured in parallel. The open circuit voltage, short-circuit current, and short-circuit charge were measured with different layers connected in parallel. All three signals increased with increasing the number of layers, shown in Fig. 3d–f. However, this might be contradictory, as voltage should have not increased when the layers are connected in parallel. This is due to the actual voltage decreased with the increase of layers, as shown in the theory is shown in Supplementary material Fig. S2 and Supplementary material Note 1. It is important to know all the tests were done at low frequencies, at 0.5 Hz, simulating the typical response of the curvature of the water wave in the ocean being low frequency. Due to the testing of the device at low frequencies, the current output is low, as the current is proportionally related to the frequency in triboelectric nanogenerators [12].

To better understand the effect of SS-TENG under horizontal motion, the SS-TENG's segment with two layer of electrode was placed on a linear motor that periodically moves the SS-TENG back and forth. The maximum displacement was set to 64 cm, and the effect of acceleration on the electrical performance of the SS-TENG due to horizontal displacement is studied. This is shown in Fig. 3a–c, for the voltage, charge, and current values. The charge, voltage, and current all increased with the acceleration due to the higher force that is applied on each of the balls moving backwards due to the horizontal motion. For small accelerations, such as at 1 m/s, the balls did not have enough kinetic energy to move from one side of the SS-TENG to the other side, showing a much lower output voltage, charge, and current.

Furthermore, multiple segments were connected, and the device's electrical output (the electric potential) are tested with only 1 layer of rolling balls with response to the number of layers under linear motor actuation, shown in Fig. 3d. The reason only 1 layer is applied is that the device voltage is high, and 2 layers would overflow the measuring system, not allowing it to be measured. With multiple segments under horizontal motion, the voltage is able to increase per each segment, and the maximum voltage is 300 V for 4 segments at an operating frequency of 1 Hz, correlating to an acceleration of 1 m/s<sup>2</sup> with the maximum displacement of 64 cm. Furthermore, the output power was measured by measuring different current for various resistance values, and the maximum power density of the device is 3.5 W/m<sup>3</sup> at the matched impedance of 120 MOhms, as shown in Fig. 3e. A segment of two layer were then placed on the linear motor, and was tested for multiple cycles, and the device output voltage is consistent over 7000 cycles, showing the device is durable and could work over thousands of cycles, as shown in Fig. 3f.

### 2.3. Theory for water effect on TENG

Furthermore, the effect of water on the device is also explored. The device was placed in a plastic container that is filled with 2 cm tall of tap water. The container was then placed on the shaker, allowing it and the device to rotate back and forth, being inclined at different angles. Fig. 4a shows that when the device is operating in water, the output voltage decreases to only 20 V if no air gap is present, while with increasing air gap, the output voltage increases as well. Once an air gap is added onto the structure with a height of 1.5 cm, the performance of the air gap structure remains the same as the device when operating in air conditions and has an output voltage of 270 V. This is because the dielectric constant of water is much larger than that of air, as shown in Supplementary material Table 1 in Supplementary Information, and the

electric field across the two electrode layers would go across the water surface, which by dielectric shielding effect, the electric field would be largely decreased. However, when the gap distance increase, the electric field would not enter the water region, and the voltage would increase with increase in the gap distance, as shown in Supplementary material Fig. S3. Finite element model simulation was also used to illustrate the effect of air gap with the structure, as shown in Supplementary material Fig. S4. This is done by having a positive charge surface on the bottom plate, illustrating the positive charges on the water surface. Also, negative charges were added on the electrode showing the charges that are induced on the electrode due to the PTFE balls moving across the surface. As the gap distance increased, the electric potential also increased, as it reached the 90% to the simulated voltage of device without any water, and this is shown in Supplementary material Fig. S5.

Also, it is important to note that in Fig. 4b, that the short-circuit output charge is the same, no matter with an air gap or without an air gap measured in water and in air. Thus, since the charge is the same, whereas the voltage decreases, it is important to know that the devices internal capacitance  $C_0$  increases by the relationship in Eq. (2), as shown in Supplementary material Fig. S3. Since the  $C_0$  is proportional to the permittivity, and water has a high permittivity  $\epsilon_r$ , and the electric field would be in the water if there is no gap; thus, causing a large increase of capacitance.

This would cause the device's output voltage would be low by Eq. (2), since the device's output charge is the same. While with an air gap, the capacitance is no longer affected by the capacitance of the water, as shown in Supplementary material Fig. S3; thus, it is able to have a higher maximum  $V_{oc}$ , while maintaining a constant short circuit charge.

Also, since the internal capacitance increase due the presence of water without an air gap structure, it is important to know that the internal resistance  $R$ , increases at the same frequency  $f$  of operation due to Eq. (3) below.

$$R_0 = \frac{1}{2\pi f C_0} \quad (3)$$

It is also seen in Fig. 4c and f that the internal resistance where we measured the relative voltage ( $V/V_{max}$ ) and output power of the device across different resistors. The resistance where the power is the maximum is the internal resistance of the device, and it decreased by 11 times (from 660 MOhms to 60 MOhms) when the device without an air gap is placed in water. This proves the fact that without an air gap structure, there would be a low voltage due to the increase of capacitance from the water, from Eq. (3), as the internal resistance decreased by 11 times, the capacitance would have to increase by 11 times, since both were operated at the same frequency of operation on the rotational shaker. This demonstrates the order of the increase in the capacitance due to the dielectric shielding effect from the water. Also, there is a significantly lower output power when the device is in water if there is no air gap present, as the power decreased from 90  $\mu$ W to 6  $\mu$ W. Also, by Eq. (3), it also explains why the internal resistance increase from 120 MOhms from Fig. 3e to 660 MOhms, as there is a frequency difference between the two sets of experiments: low frequency of operation (0.5 Hz) of the device when it is placed on the rotational shaker, as compared to the high frequency of motion from the linear motor (2 Hz), which if they have the same internal capacitance, the resistance would be lower by testing with the linear motor. Also, from the inset of Fig. 4a, with the top inset being the  $V_{oc}$  of the device with an air gap of 1.5 cm, and the bottom inset being the  $V_{oc}$  of the device with no air gap, it is clear that the  $V_{oc}$  of the device with no air gap looks like a short circuit condition. This is possibly because of the increase of the internal capacitance of the SS-TENG, decreases the internal resistance of the nanogenerator, making it have more leakage current through the represented internal capacitor of the SS-TENG, causing it to behave more like a short-circuit current condition.

The effect of salinity on the electrical output is also observed with a

device that has an air gap of 1.5 cm and a device without an air gap. The electrical performance of the device with an air gap showed the same output voltage (260 V) when the device is placed in salt water at different concentration from 0 M to 0.6 M, as shown in Fig. 4e. The latter concentration is used, because it is the concentration of salt in the ocean. However, with the air gap, the device degraded when adding more salt in the water, as the output in only water is around 40 V, and at 0.6 M, the device output voltage decreased to only 15 V, as shown in Fig. 4d, showing the device with an air gap is useful in scavenging energy from the ocean wave, while the device without an air gap's performance would decrease with increasing salt concentrations.

However, the device showed a decrease in power density without an air gap structure, due to the larger volume with an air gap. Thus, it is necessary to use the space of the air gap to increase the performance of the device. Tampered springs were added to fill the space of the air gap of 1.5 cm to increase the inclination angles of the balls for them to slide down more quickly and faster. The platform placed on ocean will incline at an angle  $\theta$  due to the curvature of the wave. For the TENG box directly placed on the platform, the inclination angle of the TENG element is  $\phi$ . For the TENG box being fixed on the platform with the spring, we denote the inclination angle of the TENG box as  $\varphi$  resulted from the ocean wave. An evaluation of the inclination angle of the platform  $\theta$  is compared to the inclination angle of the TENG element  $\phi$  is shown in Fig. 5a. Also, a spring steel mass weighing 0.4 kg was further added on top of the acrylic box structure containing the PTFE balls and electrode to increase the rotational angle of the device, as well as lowering the resonant frequency. For the TENG box connected with the spring, its inclination angle can be evaluated with the spring-mass system, as shown in Fig. 5a. Under the harmonic excitation of the ocean wave with  $\theta = \theta_0 \sin \omega t$ , the inclination angle of the TENG of the box can be written as  $\varphi = \varphi_0 \sin \omega t$ . The  $\theta_0$  and  $\varphi_0$  are the maximum amplitude of the inclination angle. With the energy conservation equation, the equation of motion of TENG box could be easily derived, as shown

in Supplementary material Note 2, and the derived equation is shown as Eq. (4) below,

$$ml^2\ddot{\varphi} - mgl \sin \varphi + k(\varphi - \theta) \left(1 - \frac{\dot{\theta}}{\dot{\varphi}}\right) = 0 \quad (4)$$

where  $g$  is the gravitational acceleration, and an overdot denotes the time differentiation. According to the real experiment, the inclination angle  $\varphi$  is not too large. Thus, by simplifying the Eq. (4), we could obtain the following nonlinear relationship below,

$$\frac{\varphi_0}{\theta_0} = \frac{1}{1 - \frac{\omega}{\omega_n} \sqrt{1 + \frac{g}{l}}} \quad (5)$$

where  $\omega_n = k/m$  is the natural frequency of the spring-mass system. It can be seen that the amplitude of the inclination angle mainly depends on the TENG's mass, the spring's stiffness and length. Thus, by using Eq. (5), Fig. 5b was derived using  $m = 1.8$  kg,  $l = 1.25$  cm, and  $k = 0.8$  N/m at different oscillating frequencies, and it shows that the  $\varphi_0$  is greater than  $\theta_0$ , showing the increase in inclination angle with the addition of the added tampered spring.

Fig. 5c shows the experimental data of the performance of the sea snake based TENG with and without a tampered spring under the actuation of the rotational shaker. With the tampered spring, the performance was enhanced by 350% at a rotation angle of 2°. This is due to, without the tampered spring, the balls could not slide down the slope all the way, at a low inclination angle of the TENG element, and with the tampered spring, the entire structure is able to be inclined at a high inclination angle and the balls are able to easily roll down and is able to have a higher maximum velocity. Also, it is important to know that without the spring, the device's output voltage would always be increasing as the inclination angle of the entire device increases from 2° to 45° by increasing the maximum rotational angle of the shaker. This is because the balls are able to slide down easily at higher inclination angle. For the device with the spring, the device's output voltage is

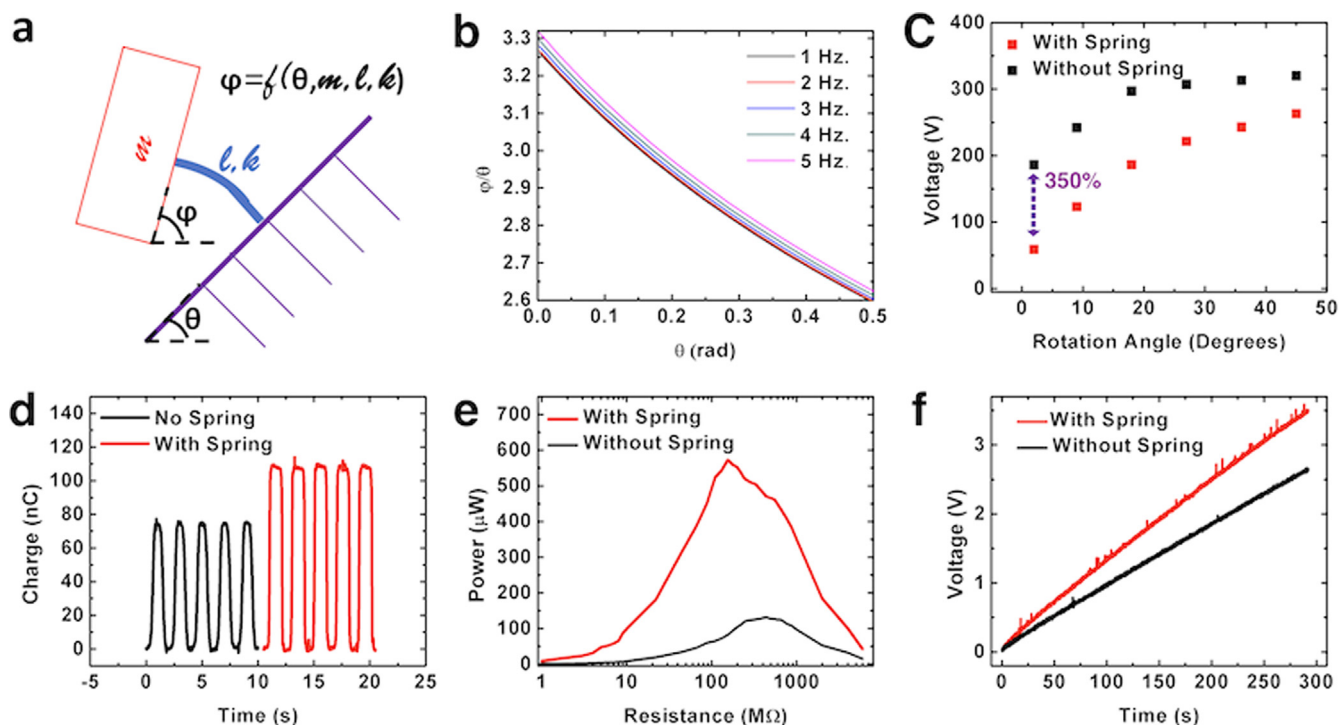


Fig. 5. Comparison of the SS-TENG without spring with SS-TENG with tampered spring by using a laboratory rocking platform. (a) Physical model of SS-TENG with spring and ANSYS simulation showing  $\phi$  dependence on  $\theta$ . (b) The simulated result of rotational angle of device with spring to original rotational angle. (c) Comparison of SS-TENG with spring and SS-TENG without spring on voltage vs rotational angle. (d) Charge vs time of SS-TENG with spring and without spring at rotational speed of 30 rpm. (e) Comparison of output power with different resistance with SS-TENG with spring and without spring. (f) Charging a 100  $\mu$ F with SS-TENG with spring and without spring on shaker with rotational speed of 30 rpm.

nearly constant for inclination angle of the entire device above an inclination angle of  $20^\circ$ , whereas for the device output without the tampered spring, the performance decrease always with decreasing rotational angle, as shown in Fig. 5c. This means that below  $20^\circ$ , the inclination angle of the TENG element is still increasing due to the restoring force on the tampered spring, and above  $20^\circ$ , the inclination angle of the balls stop increasing, and the balls reached its maximum terminal velocity. Overall, this shows that the use of the tampered spring exhibit much better performance than without a spring, especially at lower inclination angle.

Fig. 5d shows the output charge on the device when the ball is moving at the maximum inclination angle of the segment at  $45^\circ$ . The output voltage increased by nearly 150%, from 75 V to 112 V. Fig. 5e shows the output power of the device with the spring and comparing the output power of the device without the spring at the maximum inclination angle of  $45^\circ$ , and the output power is able to increase from  $100 \mu\text{W}$  to  $600 \mu\text{W}$ . This is because both charge and voltage increased with the addition of the tampered spring, which contributing to a higher power. Also, the power with the spring is at a lower resistance, thus increasing the power, as  $P = V^2/R$ . Also, the maximum power occurs at a lower resistance; this means that from Eq. (2), that the instantaneous frequency of the balls moving down would increase, which is expected, as the balls were able to move down at a higher speed due to the larger inclination angle  $\phi$  with the tampered spring. Also, the effect of charging a  $100 \mu\text{F}$  capacitor was studied, and with the spring, the capacitor was able to charge to a maximum of 3.5 V in 5 min, while without the spring, it can charge up to only 2.5 V in 5 min as shown in Fig. 5f.

#### 2.4. Demonstration

The device consists of three segments of the sea snake TENG with the attached tampered spring was then placed in our homemade water

tank made with acrylic glass. The Sea Snake TENG with the attached tampered spring was used due to its superior performance. The tank was filled with three segments in of tap water. On one end of the tank is an acrylic plate, shown in Fig. 6a, that is attached to a linear motor. The linear motor is able to be moved in a periodic motion with displacement of 8 cm and acceleration of  $2 \text{ m/s}^2$  to produce periodic water waves. Our device, which is show in the inset of Fig. 6a, in response to the periodic water waves would move up and down, similar to the COMSOL simulation as illustrated in Supplementary Video S1. It is important that we studied the effect of number of segment on the output voltage of the device, because the added springs are able to add a balance force, which greatly increase the inclination angle of the segment and the horizontal motion of the device, creating a coupled structure. This is shown in Fig. 6b, as with taken from the output of one segment of the TENG, the output voltage is only 55 V, whereas with 2 and 3 segments connected, the output voltage is greatly enhanced to 160 V, and this is due to the spring force by adding the springs. The maximum angle of the large box under the horizontal motion of water waves is around  $10^\circ$ , and we could expect the output voltage to be lower under shaker actuation, when the applied angle is  $45^\circ$ . Also, due to the periodic motion, the balls would be able to slide back and forth, producing a high voltage. The voltage was able to light 152 LED lights connected in series, which showed the phrase “Blue Energy Dream” as shown in Fig. 6c and Supplementary Video S2, and this was done without the use of a capacitor to help with the energy accumulation.

Supplementary material related to this article can be found online at <http://dx.doi.org/10.1016/j.nanoen.2018.03.062>.

Also, the effect of charging the capacitor is explored, and one device is able to charge a  $100 \mu\text{F}$  capacitor in to 2 V in 10 min, which took longer time than in Fig. 5f, due to the decrease in the inclination angle, as the box is only able to incline by  $10^\circ$  and the less impact of the wave on the device. The diagram for the circuit to charge the capacitor is show on the top left of Fig. 6c, in which there was a rectifier to only

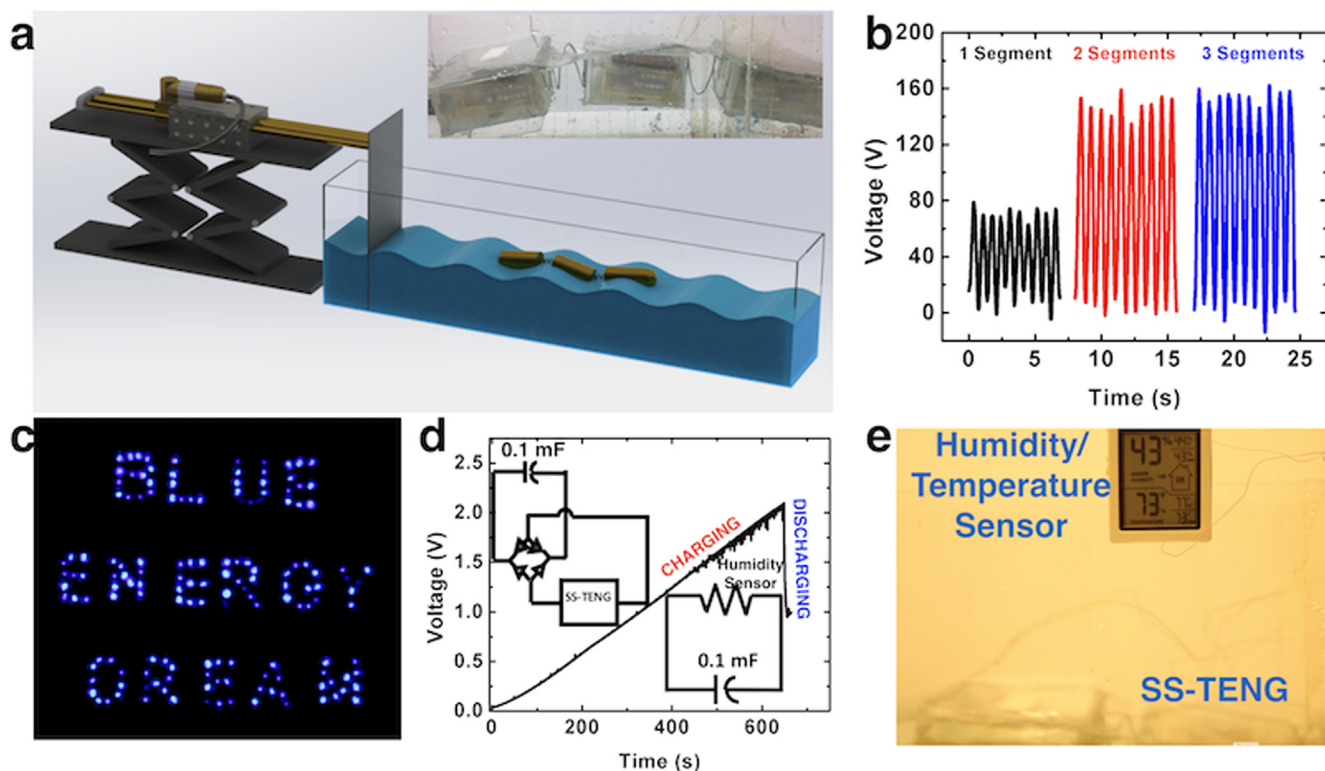


**Fig. 6.** Applications of the SS-TENG. (A) The placement of the SS-TENG in the water environment with a linear motor actuating the water waves. (b) The voltage vs time of one segment with respect to different number of segments of the SS-TENG with attached tampered spring. (c) Lighting up 152 LEDs in the words “Blue Energy Dream” with SS-TENG with attached tampered spring. (d) The charging profile of a  $100 \mu\text{F}$  capacitor by the SS-TENG in water. (e) The application of driving and powering the humidity sensor with SS-TENG with attached tampered spring.

allow current to flow in one direction connected to the SS-TENG, and then it was connected to the capacitor. Then, to power the humidity sensor, 2 V was required, and the capacitor was able to successfully power the temperature and humidity sensor, which is shown in Supplementary Video S3 and Fig. 6d.

Supplementary material related to this article can be found online at <http://dx.doi.org/10.1016/j.nanoen.2018.03.062>.

### 3. Conclusion

In summary, a sea snake based TENG based of the Pelamis wave energy converter was designed, using balls that are able to move with the structure of the sea snake. The output performance of the SS-TENG was measured using a rotational shaker to explore the effect of curvature of the wave and a linear motor to explore the effect of motor acceleration. Furthermore, the device was tested in water, and there needs to be an air gap structure to minimize the effect of water ion charges screening the output potential. With an air gap, the SS-TENG was able to operate in high salinity environment, such as simulated ocean conditions. Tampered springs have been added to fill the air gap to increase the operating angle of the device, and the device could rotate under low actuation angles, up to 2°. The sea snake based TENG was then placed in water, and the TENG was able to light up 152 lights in water, due to its air gap structure, allowing the high output voltage in water.

### 4. Experimental section

#### 4.1. Fabrication of the SS-TENG

The SS-TENG is fabricated by first fabricated by bonding a acrylic mask with interdigital electrode on top of another acrylic sheet (1/16"). The structure was then deposited with copper by using PVD Sputtering technique (Kurt J. Leskar PVD 75). The mask was then removed, and a wire connecting to the copper layer is added. Then, a thin film of nylon was placed over the acrylic with Cu interdigital electrode. Then, an acrylic separator was added to separate the columns, and 6 PTFE balls were placed in each column. This was repeated multiple times, to get multiple layers, and the device is then fully enclosed in an acrylic box. Then, a larger acrylic box is created with an opening on the top, and a tampered spring was cut and bonded to the bottom of the larger box on one side, and to the bottom of smaller box containing the PTFE balls. The spring steel is added on top of the smaller box, and the larger acrylic box structure is enclosed. Springs were then connected to other big boxes containing the structure to create the SS-TENG.

#### 4.2. Electrical measurement of the TENG

The electric output, such as open-circuit voltage, short circuit charge and short circuit current signals were measured by the Keithley 6514 System Electrometer. The external forces were applied by a rotational shaker (Benchmark Scientific BR2000 BenchRocker 2D Variable Speed Platform Rocker), or a linear motor. For Fig. 6, the SS-TENG was placed in a homemade water tank, with a linear motor creating water waves, triggering the SS-TENG.

### Acknowledgements

The authors are grateful for the support received from the National Key Research and Development Program of China (No. 2016YFA0202704), the "Thousands Talents" program for pioneer researcher and his innovation team in China, the National Natural Science Foundation of China (Nos. 51506019, 11672265 and 11621062), the Young Elite Scientists Sponsorship Program by CAST (2016QNR001).

### Conflict of interest

The authors declare no conflict of interest.

### Appendix A. Supplementary material

Supplementary data associated with this article can be found in the online version at <http://dx.doi.org/10.1016/j.nanoen.2018.03.062>.

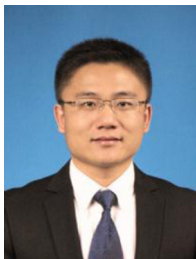
### References

- [1] D. Gielen, F. Boshell, D. Saygin, *Nat. Mater.* 15 (2016) 117.
- [2] S. Chu, A. Majumdar, *Nature* 488 (2012) 294.
- [3] S. Chu, Y. Cui, N. Liu, *Nat. Mater.* 16 (2016) 16.
- [4] A. Clément, P. McCullen, A. Falcão, A. Fiorentino, F. Gardner, K. Hammarlund, G. Lemonis, T. Lewis, K. Nielsen, S. Petroncini, M.T. Pontes, P. Schild, B.-O. Sjöström, H.C. Sørensen, T. Thorpe, *Renew. Sustain. Energy Rev.* 6 (2002) 405.
- [5] J. Tollefson, *Nature* 508 (2014) 302.
- [6] E. Callaway, *Nature* 450 (2007) 156.
- [7] Z.L. Wang, T. Jiang, L. Xu, *Nano Energy* 39 (2017) 9.
- [8] Z.L. Wang, *Nature* 542 (2017) 159.
- [9] J. Chen, J. Yang, Z. Li, X. Fan, Y. Zi, Q. Jing, H. Guo, Z. Wen, K.C. Pradel, S. Niu, Z.L. Wang, *ACS Nano* 9 (2015) 3324.
- [10] A.F.d.O. Falcão, *Renew. Sustain. Energy Rev.* 14 (2010) 899.
- [11] J. Falmes, *Mar. Struct.* 20 (2007) 185.
- [12] Y.L. Zi, H.Y. Guo, Z. Wen, M.H. Yeh, C.G. Hu, Z.L. Wang, *ACS Nano* 10 (2016) 4797.
- [13] Z.L. Wang, *Faraday Discuss.* 176 (2014) 447.
- [14] Z.L. Wang, J. Chen, L. Lin, *Energy Environ. Sci.* 8 (2015) 2250.
- [15] M. Xu, Y.-C. Wang, S.L. Zhang, W. Ding, J. Cheng, X. He, P. Zhang, Z. Wang, X. Pan, Z.L. Wang, *Extrem. Mech. Lett.* 15 (2017) 122.
- [16] S.L. Zhang, Y.-C. Lai, X. He, R. Liu, Y. Zi, Z.L. Wang, *Adv. Funct. Mater.* 27 (2017) 1606695.
- [17] S. Wang, X. Wang, Z.L. Wang, Y. Yang, *ACS Nano* 10 (2016) 5696.
- [18] S. Wang, X. Mu, X. Wang, A.Y. Gu, Z.L. Wang, Y. Yang, *ACS Nano* 9 (2015) 9554.
- [19] Y.C. Lai, J. Deng, S. Niu, W. Peng, C. Wu, R. Liu, Z. Wen, Z.L. Wang, *Adv. Mater.* 28 (2016) 10024.
- [20] Z. Zhao, X. Pu, C. Du, L. Li, C. Jiang, W. Hu, Z.L. Wang, *ACS Nano* 10 (2016) 1780.
- [21] X. Wang, Z. Wen, H. Guo, C. Wu, X. He, L. Lin, X. Cao, Z.L. Wang, *ACS Nano* 10 (2016) 11369.
- [22] Z. Wen, H. Guo, Y. Zi, M.H. Yeh, X. Wang, J. Deng, J. Wang, S. Li, C. Hu, L. Zhu, Z.L. Wang, *ACS Nano* 10 (2016) 6526.
- [23] H. Shao, Z. Wen, P. Cheng, N. Sun, Q. Shen, C. Zhou, M. Peng, Y. Yang, X. Xie, X. Sun, *Nano Energy* 39 (2017) 608.
- [24] Y. Xi, H. Guo, Y. Zi, X. Li, J. Wang, J. Deng, S. Li, C. Hu, X. Cao, Z.L. Wang, *Adv. Energy Mater.* 7 (2017) 1602397.
- [25] T. Jiang, Y. Yao, L. Xu, L. Zhang, T. Xiao, Z.L. Wang, *Nano Energy* 31 (2017) 560.
- [26] J. Wang, S. Li, F. Yi, Y. Zi, J. Lin, X. Wang, Y. Xu, Z.L. Wang, *Nat. Commun.* 7 (2016) 12744.
- [27] Y. Yang, G. Zhu, H. Zhang, J. Chen, X. Zhong, Z.H. Lin, Y. Su, P. Bai, X. Wen, Z.L. Wang, *ACS Nano* 7 (2013) 9461.
- [28] K. Dong, J. Deng, Y. Zi, Y.-C. Wang, C. Xu, H. Zou, W. Ding, Y. Dai, B. Gu, B. Sun, Z.L. Wang, *Adv. Mater.* 29 (2017) 1702648.
- [29] K. Dong, Y.-C. Wang, J. Deng, Y. Dai, S.L. Zhang, H. Zou, B. Gu, B. Sun, Z.L. Wang, *ACS Nano* 11 (2017) 9490.
- [30] M. Xu, P. Wang, Y.-C. Wang, S.L. Zhang, A.C. Wang, C. Zhang, Z. Wang, X. Pan, Z.L. Wang, *Adv. Energy Mater.* (2017) 1702432.
- [31] H.S. Wang, C.K. Jeong, M.-H. Seo, D.J. Joe, J.H. Han, J.-B. Yoon, K.J. Lee, *Nano Energy* 35 (2017) 415.
- [32] C. Dagdeviren, P. Joe, O.L. Tuzman, K.-I. Park, K.J. Lee, Y. Shi, Y. Huang, J.A. Rogers, *Extrem. Mech. Lett.* 9 (2016) 269.
- [33] L. Pan, J. Wang, P. Wang, R. Gao, Y.-C. Wang, X. Zhang, J.-J. Zou, Z.L. Wang, *Nano Res.* (2018), <http://dx.doi.org/10.1007/s12274-018-1989-9>.
- [34] C. Xu, Y. Zi, A.C. Wang, H. Zou, Y. Dai, X. He, P. Wang, Y.-C. Wang, P. Feng, D. Li, Z.L. Wang, *Adv. Mater.* (2018) 1706790, <http://dx.doi.org/10.1002/adma.201706790>.
- [35] R. Liu, X. Kuang, J. Deng, Y.-C. Wang, A.C. Wang, W. Ding, Y.-C. Lai, J. Chen, P. Wang, Z. Lin, H.J. Qi, B. Sun, Z.L. Wang, *Adv. Mater.* 30 (2018) 1705195.
- [36] Z.L. Wang, *Mater. Today* 20 (2017) 74.
- [37] C. Zhang, W. Tang, C.B. Han, F.R. Fan, Z.L. Wang, *Adv. Mater.* 26 (2014) 3580.
- [38] G. Zhu, Y.J. Su, P. Bai, J. Chen, Q.S. Jing, W.Q. Yang, Z.L. Wang, *ACS Nano* 8 (2014) 6031.
- [39] Y.J. Su, X.N. Wen, G. Zhu, J. Yang, J. Chen, P. Bai, Z.M. Wu, Y.D. Jiang, Z.L. Wang, *Nano Energy* 9 (2014) 186.
- [40] L. Xu, Y.K. Pang, C. Zhang, T. Jiang, X.Y. Chen, J.J. Luo, W. Tang, X. Cao, Z.L. Wang, *Nano Energy* 31 (2017) 351.
- [41] Z.H. Lin, G. Cheng, X.H. Li, P.K. Yang, X.N. Wen, Z.L. Wang, *Nano Energy* 15 (2015) 256.
- [42] A. Ahmed, Z. Saadatnia, I. Hassan, Y.L. Zi, Y. Xi, X. He, J. Zu, Z.L. Wang, *Adv. Energy Mater.* 7 (2017).
- [43] B. Drew, A.R. Plummer, M.N. Sahinkaya, Sage Publications Sage, London, England UK, 2009.
- [44] R. Gobato, A. Gobato, D.F.G. Fedrigo, *arXiv preprint arXiv:1508.01106*, 2015.

[45] S. Niu, Y. Liu, X. Chen, S. Wang, Y.S. Zhou, L. Lin, Y. Xie, Z.L. Wang, *Nano Energy* 12 (2015) 760.



**Steven L. Zhang** received his B.S. degree in Electronic Materials Engineering from U.C. Davis in 2014. He is currently pursuing a Ph.D. in Material Science and Engineering at Georgia Institute of Technology, and is working for Dr. Zhong Lin Wang. His research focuses on nanogenerators, energy harvesting, and self-powered active sensing.



**Dr. Minyi Xu** received his Ph.D. degree from Peking University in 2012. Now he is an Associate Professor in the Marine Engineering College, Dalian Maritime University. His current research is mainly focused on the areas of triboelectric nanogenerators and its practical applications in smart ship and ocean.



**Dr. Chunli Zhang** received his Ph.D. (2011) in Structural Engineering from Zhejiang University, China. Then he joined the group of Professor Chuanzeng Zhang at the University of Siegen as a postdoctoral fellow. He is currently an associate Professor at Zhejiang University since 2014. In 2017, he joined in the group of Professor Zhonglin Wang at the Georgia Institute of Technology. His main research interests are mechanics of smart materials/structures, mechanics of multiferroic materials/structures, and analysis of piezoelectric/piezotronic/piezo-photonic devices.



**Dr. Yi-Cheng Wang** is currently a postdoctoral researcher in the School of Materials Science and Engineering at Georgia Institute of Technology, working alongside Dr. Zhong Lin Wang. Yi-Cheng's research interests include the synthesis and application of advanced materials for sensors and energy devices. He received his M.S. in Chemistry and Ph.D. in Biological Systems Engineering from University of Wisconsin-Madison, and holds a B.S. in Bio-Industrial Mechatronics Engineering from National Taiwan University. He was a National Science Foundation Scholar in Green Chemistry in 2013, and his other awards and honors include a Wisconsin Distinguished Graduate Fellowship.



**Haiyang Zou** received his M.S. degree in Worcester Polytechnic Institute, United States in 2012 and B.S. degree in Nanchang University, China in 2010. He is currently a Ph.D. candidate in Georgia Institute of Technology under the supervision of Prof. Zhong Lin Wang. Haiyang's research interests include energy nanomaterials, nano-systems and nano-devices; piezo-electronics and piezo-optoelectronics, flexible electronics.



**Dr. Xu He** received his B.S. in Polymer Materials and Engineering, M.S. in Materials Science, and Ph.D. in Materials Science from Sichuan University in 2010, 2014, and 2017, respectively. He was a joint Ph.D. student in Materials Science and Engineering at Georgia Institute of Technology during 2015–2017 under the supervision of Prof. Zhong Lin Wang through the program of China Scholarship Council (CSC). His research focuses primarily on nanomaterials fabrication, nanostructure design and the modification of polymers for functional bio-nanocomposites, energy harvesting/storage, active sensing systems and flexible electronics devices.



**Dr. Zhengjun Wang** obtained bachelor degree and Ph.D. both in physics from Henan Normal University and West Virginia University, respectively. He is currently a Postdoctoral Fellow in Prof. Zhong Lin Wang's group at Georgia Institute of Technology, his research interests focus on fabrication of nanoelectronic devices and triboelectric nanogenerators.



**Zhong Lin Wang** received his Ph.D. from Arizona State University in physics. He now is the Hightower Chair in Materials Science and Engineering, Regents' Professor, Engineering Distinguished Professor and Director, Center for Nanostructure Characterization, at Georgia Tech. Dr. Wang has made original and innovative contributions to the synthesis, discovery, characterization and understanding of fundamental physical properties of oxide nanobelts and nanowires, as well as applications of nanowires in energy sciences, electronics, optoelectronics and biological science. His discovery and breakthroughs in developing nanogenerators established the principle and technological road map for harvesting mechanical energy from environment and biological systems for powering personal electronics. His research on selfpowered nanosystems has inspired the worldwide effort in academia and industry for studying energy for micro-nano-systems, which is now a distinct disciplinary in energy research and future sensor networks. He coined and pioneered the field of piezotronics and piezo-phototronics by introducing piezoelectric potential gated charge transport process in fabricating new electronic and optoelectronic devices. Details can be found at: <http://www.nanoscience.gatech.edu>.